# An AFM/STM multi-mode nanofabrication approach allowing *in situ* surface modification and characterisation

*Weihua Hu*[1], *J. Bain*[2], *D. Ricketts*[3]

[1]*Department of Physics, Carnegie Mellon University, Pittsburgh, PA 15213, USA*
[2]*Department of Electrical and Computer Engineering, Carnegie Mellon University, Pittsburgh, PA 15213, USA*
[3]*Department of Electrical and Computer Engineering, North Carolina State University, Raleigh, NC 27606, USA*
*E-mail: weihuahu86@gmail.com*

Published in Micro & Nano Letters; Received on 4th November 2012; Accepted on 8th January 2013

A report is presented on a new multi-mode nanofabrication method that uses a compliant conductive atomic force microscope (AFM) probe for both AFM and scanning tunnelling microscope (STM) operation and it is demonstrated that these modes can be switched 'on-the-fly' during the measurement or fabrication of nanostructures. The authors oxidised Ti with the same conductive AFM probe in AFM and STM modes, alternately in a continuous writing step. An in-plane Ti—$TiO_x$—Ti junction was fabricated by combining AFM and STM modes and electrically characterised by taking current images in conductive AFM mode. After measurement, additional features were written to increase the electrical isolation, thus realising *in situ* nanoscale modification.

**1. Introduction:** Scanning probe microscopy (SPM) has played a key role in our understanding and manipulation of matter at the nanometre scale. Scanning tunnelling microscopy (STM) and atomic force microscopy (AFM) are two principal modalities of SPM that have been extensively used for both measurement and for surface modification and nanofabrication [1, 2]. STM offers very high lateral and vertical resolution and operates without contact to the substrate; it does, however, require a conductive substrate that limits its application in many areas [3, 4]. AFM also provides high vertical resolution, but requires contact or very close proximity to the substrate; it, however, is able to operate on either insulating or conductive substrates [4, 5]. Both modalities have been leveraged for fabrication as well as the measurement of nanometre-scale systems. For example, both AFM- and STM-based local oxidation have been widely applied in fabricating nanostructures and nanodevices [6—9] using Ti substrates, which are readily oxidised in the presence of water and an electric field between the tip and surface. AFM-based oxidation has been used to fabricate relatively wider features in comparison with STM. For Ti oxidation in our group, the minimum size oxide feature produced by AFM-mode local oxidation is an approximately 50 nm-wide line, whereas STM-mode local oxidation using standard Pt/Ir STM tips has produced 10 nm-wide oxidation features [10].

Several different devices have been realised using tip-directed nano oxidation, such as single-electron transistors [11] and metal—insulator—metal (MIM) diodes [12]. Common to these devices is the need to fabricate very small features, ideally with nanometre accuracy, which electrically isolates adjacent conducting regions. For the highest resolution, STM is the optimal modality. For operation on insulating areas, AFM is required. Ideally, we would like to achieve nanofabrication using both modalities, switching between the two as required by the device structure.

In this Letter, we demonstrate dual STM/AFM-mode operation by using a compliant conductive AFM probe with both tunnelling current and displacement feedback. The term 'AFM probe' is used to refer to the whole body of an AFM cantilever including the sharp tip at its end. In this Letter, an AFM probe will be used as an end-effector to replace the more traditional, essentially rigid, STM tip used in STM mode. Since both feedback modalities are present during operation, we are able to switch between modalities 'on-the-fly', allowing us to optimise modality for the specific feature being fabricated. In addition, the compliance of the probe in our approach makes possible local control of the probe displacement via a local actuator. Such tip-height control on a probe-by-probe basis enables our work to be extended in the future to large arrays of SPM probes operating in parallel for large-scale nanofabrication [10].

We begin by demonstrating multi-mode SPM nanofabrication by locally oxidising Ti in AFM and STM modes, alternately, with the same conductive AFM probe. In this Letter, the specific mode of AFM operation was contact AFM mode and we use 'AFM mode' for simplicity. During fabrication, we switched between the two modes 'on-the-fly'. Then, we fabricated MIM junctions by using the conductive AFM probes in multi-mode operation: (i) AFM mode for topographical, current imaging and coarse oxide feature writing and (ii) STM mode for fine feature oxide writing. STM mode writing enabled significantly finer features than AFM mode, whereas AFM mode enabled imaging and metrology on and near the insulating regions of the substrate. In addition, we electrically characterised the fabricated MIM junction, *in situ*, by applying a bias voltage between the conductive AFM probe and the sample and measuring the current that flows. Finally, we show that with multi-mode operation and *in situ* characterisation, we were able to modify the fabricated MIM junctions immediately following electrical characterisation of the written feature by adding a second oxidation line and thus increasing the electrical isolation. This approach would allow features to be written and rewritten until a particular electrical property was reached.

**2. Experimental:** Ti layers with a thickness of 5 nm were deposited using an electron beam evaporator at a base pressure of $2 \times 10^{-10}$ torr on a 1 μm-thick $SiO_2$ layer, which, in turn, was on top of an Si substrate. The $SiO_2$ served as the electrical insulation for the Ti structures deposited [13]. The Ti layers were patterned into 2 μm-wide strips using photolithography (lift-off) with a length of 80 μm. All strips were electrically connected at one (common) end with the other ends isolated. Sputtered Au contact pads with a thickness of 200 nm were deposited by lift-off at the ends of the Ti strip, both on the common and the isolated ends. The large common pad was connected to the SPM stage using a metal clip, permitting an electrical current path for oxidation as well as conductive AFM imaging.

The SPM used for the experiments was an ATM 350 ambient SPM system designed and manufactured by RHK Technology (Troy, MI, USA). Two types of conductive AFM probes were

used for both AFM mode and STM mode oxidation. One probe was an antimony (n)-doped silicon probe with Pt/Ir coating (Bruker, SCM-PIT) with a cantilever spring constant between 1 and 5 N/m. This probe was used multi-mode operation with on-the-fly mode switching and also for MIM junction fabrication. However, it was not reliable for current imaging because of the low wear resistance of the tip. The other probe used was an antimony (n)-doped silicon probe with a diamond-coated tip (Bruker, DDESP) with a cantilever spring constant of between 20 and 80 N/m. This probe has increased wear resistance and was utilised for both fabricating MIM junctions and electrical measurement. The experimental setup for the multi-mode operation is shown in Fig. 1*a*, and the target MIM structure is shown in Fig. 1*b*.

As seen from Fig. 1*a*, the conductive, compliant AFM probe, which was electrically connected to the control system, worked as an end-effector for both AFM and STM modes. When working in AFM mode, the optical deflection signal was used as the feedback control signal; when working in STM mode, the tunnelling current signal was used as the feedback control signal [10, 13].

The SPM local oxidation experiment was performed in an ambient environment at room temperature with a relative humidity of 40—45%. The Pt/Ir-coated AFM probe was used to locally oxidise Ti along a line on a 5 nm-thick Ti film. A $TiO_x$ line was fabricated in four sections, where the modality of the SPM was switched between AFM and STM modes. After the oxidation of one section the probe tip was stopped, held in place and the modality of the SPM switched. Then the tip continued along the line, writing in the new modality. The first and third segments were oxidised in AFM mode and the second and fourth segments were oxidised in STM mode. In AFM mode, the Ti layer was biased at +10 V relative to the probe as shown in Fig. 1*a* and the tip-scanning rate was 10 nm/s. The bias of +10 V on the Ti layer was the minimum bias that was able to oxidise Ti reliably in AFM mode in our system. In STM mode, the Ti layer was biased at +3.5 V, which was the minimum bias voltage for STM mode oxidation, and the current setpoint was set at 1.5 nA and the tip-scanning rate to 10 nm/s. After fabrication, a topographical image was taken in AFM mode with the same probe. Similarly, a '*C*' shape structure was also fabricated in this multi-mode method to illustrate the ability to write arbitrary features and a topographical AFM image was taken after fabrication.

An MIM structure was fabricated on a 2 µm-wide Ti strip. To achieve the minimum width insulating region, STM mode was used to write a line across most of the strip width. To ensure electrical isolation, AFM mode was used to extend this STM-written insulating line to the edges of the Ti strip, since STM mode will not operate near the edge owing to the insulating nature of the $SiO_2$ on the sample. The features were written in an ambient environment at room temperature with the relative humidity of 20—25%. The experimental procedure was as follows. First, a $3.3 \times 3.3$ µm area was scanned using AFM mode to find the Ti strip. AFM mode was chosen rather than STM mode because of the insulating field of $SiO_2$ surrounding the Ti strips, which does not support STM operation. Then, the probe was moved to the Ti layer, which is conductive and the operation mode was switched to STM mode. This mode (STM) was used for positioning the probe tip at the target site for STM writing. Positioning under STM without writing is done with the Ti layer biased at +2 V and the current setpoint set at 0.5 nA; these parameters prevent oxidation from occurring during positioning. To write the centre line under STM mode, the bias on the Ti was increased to +3.5 V and the current setpoint was to 1.5 nA. The tip was moved along an 800 nm line path in the centre of the Ti strip at the speed of 10 nm/s.

After oxidising the 800 nm Ti line in the centre, the operation mode was changed back to AFM mode. The area between the previously STM-oxidised line and the strip edge were oxidised by scanning the two regions in AFM mode at the speed of 1 µm/s with the Ti layer biased at +10 V. These scanned areas were large enough to ensure the oxidation across the entire Ti strip in order to form a complete lateral MIM junction. After each oxidation step, the $3.3 \times 3.3$ µm area was scanned in conductive AFM mode, which allows topographical information to be collected simultaneously with maps of the current conducted through the tip at each location. In conductive AFM mode, the sample was biased at −1 V to allow imaging while preventing oxidation because of the negative bias. This step is particularly useful since it allows us to investigate the electrical fidelity of the written structures, and if necessary, re-write them.

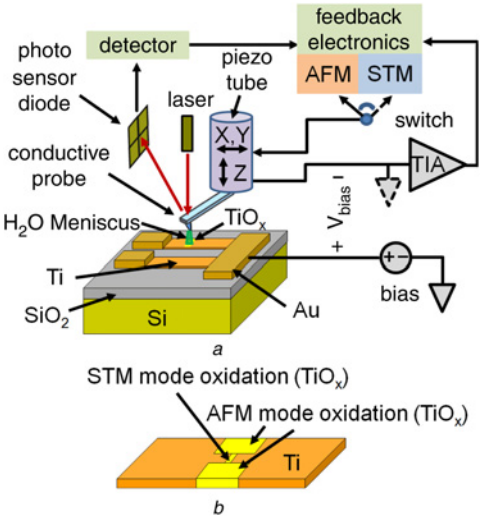


**Figure 1** *Schematic diagram of experimental apparatus used in this work, and structure of tip-oxidised lateral MIM junction*
*a* Schematic diagram of experimental apparatus used in this work
A conductive AFM probe was employed in AFM, conductive AFM and STM modes. The feedback signal while in AFM and conductive AFM modes are optical detection signal, whereas feedback signal in STM mode is tunnelling current. $V_{bias}$ is potential between bias supply and probe, which is held at virtual ground, as shown by dashed ground symbol, by the transimpedance amplifier (TIA)
*b* Structure of tip-oxidised lateral MIM junction

**3. Results and discussion:** Fig. 2 shows the AFM images of $TiO_x$ structures fabricated using AFM and STM modes alternately with a Pt/Ir AFM probe. The switch between the two modes occurred without disengaging the tip, and thus the fabricated $TiO_x$ structures appear as a continuous feature, with each segment having different widths and heights corresponding to the different fabrication modes. Fig. 2*a* displays a four-segment $TiO_x$ structure

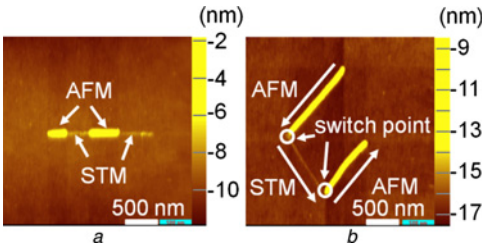


**Figure 2** *Topographical AFM image of $TiO_x$ chain of four segments in line, and topography AFM image of $TiO_x$ structure of three segments in '*C*' shape*
*a* Topographical AFM image of $TiO_x$ chain of four segments in line
The two wider sections fabricated in AFM mode, whereas other two fabricated in STM mode
*b* Topography AFM image of $TiO_x$ structure of three segments in '*C*' shape
The two wider lines fabricated in AFM mode, whereas middle line fabricated in STM mode




doi: 10.1049/mnl.2012.0859

with the segments in a straight line. Fig. 2*b* shows a three-segment $TiO_x$ structure in a '*C*' shape. Although the feedback mode must change from cantilever deflection to tunnelling current, no obvious shift in position or feature occurs at the transition.

Fig. 3 shows the topographical images of an MIM junction fabricated in multi-mode SPM local oxidation using a Pt/Ir-coated AFM probe. Fig. 3*b* shows the zoomed-in view of the STM oxidised line in the centre, which was <20 nm wide. However, the disadvantage of this type of probes was that the Pt/Ir coating was only 20 nm thick, so it was very easily worn away during AFM scanning and thus was not reliable for current imaging in conductive AFM operation.

To increase wear resistance of the tip and thus enable reliable conductive AFM operation, a diamond-coated conductive AFM probe was used. The doped diamond coating increased the lifetime of the tip but the trade-off was that it has a larger tip diameter. Fig. 4 shows the multi-mode SPM local oxidation results using a diamond-coated conductive AFM probe. Figs. 4*a*—*e* show the topographical images for each state during the experiment and Figs. 4*f*—*j* show the corresponding current images. The images of Fig. 4 were taken in conductive AFM mode as described above with the −1 V bias applied. The series resistance of the Ti strip is 10—50 kΩ, such that the maximum current that will flow while imaging under a −1 V bias should be between 20 and 100 μA. The current reading in those unoxidised regions, however, did not reach 20 μA and did not even reach 100 nA, the saturation level of the amplifier, because of the native oxidation layer on the Ti surface. After the STM mode oxidised line and AFM mode oxidised pads were formed [Fig. 4*d*], the current image was taken, Fig. 4*i*. No obvious decrease of the current was seen on the left side of the MIM junction, which indicated that electrical isolation was not achieved. This STM oxidation line was wider than the one oxidised with the Pt/Ir-coated AFM probe as shown in Fig. 3, because the diamond-coated tip had larger radius. To illustrate the power of the multi-mode fabrication approach, another oxidation line was written by the same probe in AFM mode at the speed of 10 nm/s, whereas the Ti strip was biased at +10 V. The AFM oxidation line (left line in Fig. 4*e*) was wider than the STM oxidation line (right line in Fig. 4*e*). As seen in Fig. 4*j*, current on the left side of the MIM junction decreased dramatically after the AFM oxidation line was written, which indicates that the electrical isolation was improved by adding the AFM oxidised line. We calculated the resistance of the oxidation line using the current images by simply subtracting the resistance of the right-hand side of the MIM junction from the left-hand side of the MIM junction. Assuming the oxidation totally penetrated through the Ti layer [11, 13], the resistivity of the oxidised lines in both AFM and STM modes were estimated by assuming that current flowed across the width of the written lines and is uniformly distributed through the thickness and along the length of the lines. The resistivity of the oxide in the STM-oxidised line was thus estimated at 6.7 Ω-m compared with 40 Ω-m estimated for the material in the AFM oxidised line. For comparison, the resistivity of crystalline forms of $TiO_2$ is about $10^{11}$ Ω-m at room temperature [14] and the resistivity of nano-$TiO_2$ particles is about $1.6 \times 10^4$ Ω-m as reported [15]. The $TiO_x$ features oxidised in both STM and AFM modes are much less resistive than $TiO_2$ in both crystalline and nanoparticle forms.

Topographical cross-sections after the completion of the entire writing process of Fig. 4 are shown in Fig. 5. The blue solid line shows the AFM oxidised regions are 2 nm higher than the Ti layer and by comparing the green dashed line and the blue solid line it is seen that the STM oxidised line is 1 nm less than the

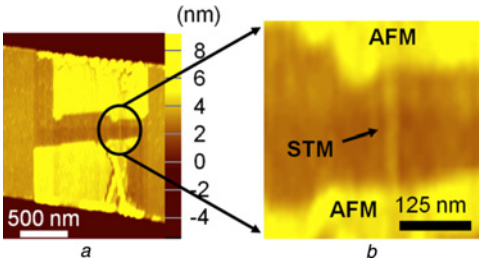


**Figure 3** *Topographical AFM image of MIM junction after tip-oxidation using Pt/Ir-coated conductive AFM probe in multi-mode, and zoomed-in image of STM oxidation line*
*a* Topographical AFM image of MIM junction after tip-oxidation using Pt/Ir-coated conductive AFM probe (Bruker, SCM-PIT) in multi-mode
Radius of tip is about 20—25 nm. Thin line in centre was the oxidation line fabricated in STM mode and the two big pads at its ends were oxidised in AFM mode. Width of oxidation line is thinner than 20 nm
*b* Zoomed-in image of STM oxidation line

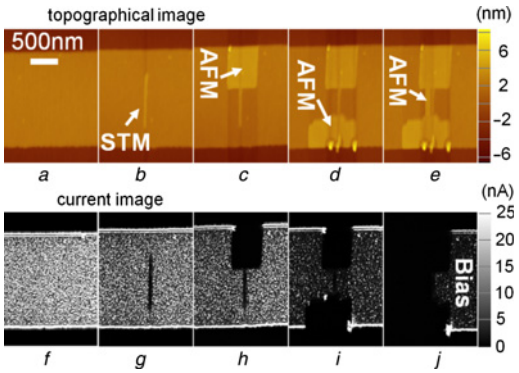


**Figure 4** *Multi-mode SPM local oxidation results with diamond-coated AFM probes (Bruker, DDESP)*
Tip radius of AFM probe is about 35—50 nm
*a*—*e* Topographical images for each state during multi-mode SPM local oxidation
*f*—*j* Corresponding current images: *a*, *f* before oxidising; *b*, *g* after first line oxidised in STM mode; *c*, *h* after top square oxidised in AFM mode; *d*, *i* after second square oxidised in AFM mode; *e*, *j* after second line oxidised in AFM mode. Bias voltage applied on right side of Ti layer as shown by *j*

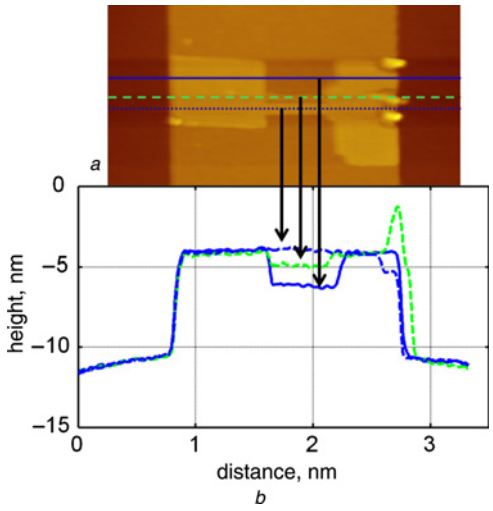


**Figure 5** *Topographical image of MIM junction with both STM and AFM oxidised lines, and cross-section views for three places*
*a* Topographical image of MIM junction with both STM and AFM oxidised lines
Three lines with different colours or styles show the three places to cut through for cross-section views
*b* Cross-section views for three place
(1) Blue solid line shows cross-section through two AFM oxidised pads and unoxidised Ti layer in middle; (2) green dashed line shows cross-section through two AFM oxidised pads and STM oxidised line; (3) blue dashed line shows cross-section through two AFM oxidised pads and AFM oxidised line

AFM oxidised features in height. This reduced topographical height indicates a lower degree of oxidation in STM mode than in AFM mode, since the incorporation of oxygen increases the volume of material as oxidation is more complete [16].

**4. Summary and conclusions:** Multi-mode SPM local oxidation of Ti was achieved, in which $TiO_x$ structures of linked segments were fabricated by using AFM and STM modes alternately while switching 'on-the-fly' between the two modes. An MIM structure was fabricated by using conductive AFM probes in STM and AFM modes. In addition to the ability to both fabricate nanostructures and characterise, the created nanopatterns *in situ* were also shown. Finally, we achieved *in situ* nanomodification by further oxidising the created MIM structures. All the nanofabrication, electrical characterisation and nanomodification were achieved with the same probe and were sequential operations. There are four main advantages of implementing multi-mode SPM-based nanofabrication: (i) smaller tip-oxidation features can be produced using STM mode; (ii) AFM mode allows tip operation on electrically isolated features and insulating substrates, permitting fabrication at the interface of conducting/insulating regions; (iii) conductive AFM enables *in situ* electrical characterisation during the nanofabrication and thus paves the way for further *in situ* nanomodification; and (iv) using compliant AFM probes will enable individual actuation for use in future arrays [10, 17], which will significantly increase nanofabrication throughput.

**5. Acknowledgments:** The authors acknowledge TFAN group members G. Fedder, L. Carley, R. Davis, O. Ozcan, Y. Dang, Y. Zhang and Y. Tang for invaluable discussions. This work was supported by the DARPA Tip Based Nanofabrication Program (grant no. N66001-08-1-2039).

## 6 References

[1] Stroscio J.A., Eigler D.M.: 'Atomic and molecular manipulation with the scanning tunneling microscope', *Science*, **254**, (5036), pp. 1319—1326

[2] Marrian C.R.K., (Ed.): 'Technoglogy of proximal probe lithography' (SPIE, Bellingham, WA, 1993)

[3] Binnig G., Rohrer H.: 'Scanning tunneling microscopy', *Surf. Sci.*, **126**, (1), 1983, pp. 236—244

[4] Kalinin S., Gruverman A.: 'Scanning probe microscopy' (Springer, 2007)

[5] Binnig G., Quate C.F., Gerber Ch.: 'Atomic force microscope', *Phys. Rev. Lett.*, 1986, **56**, (9), pp. 930—933

[6] Dagata J.: 'Device fabrication by scanned probe oxidation', *Science*, 1995, **270**, (5242), pp. 1625—1626

[7] Snow E., Campbell P.: 'AFM fabrication of sub-10-nanometer metal-oxide devices with in situ control of electrical properties', *Science*, 1995, **270**, (5242), pp. 1639—1641

[8] Matsumoto K., Takahashi S., Ishii M., *ET AL.*: 'Application of STM nanometer-size oxidation process to planar-type MIM diode', *Japan. J. Appl. Phys.*, 1995, **34**, (1), pp. 1387—1390

[9] Snow E., Campbell P.: 'Fabrication of Si nanostructures with an atomic force microscope', *Appl. Phys. Lett.*, 1994, **64**, (15), pp. 1932—1934

[10] Hu W., Tang Y., Zhang Y., *ET AL.*: 'Ti/$TiO_2$ nanodevices fabrication using compliant probes and CMOS probe-arrays'. Proc. Technologies for Future Micro/Nano Manufacturing, Napa, CA, USA, August 2011

[11] Matsumoto K., Ishii M., Segawa K., Oka Y., Vartanian B., Harris J.: 'Room temperature operation of a single electron transistor made by the scanning tunneling microscope nanooxidation process for the $TiO_x$/Ti system', *Appl. Phys. Lett.*, 1996, **68**, (1), pp. 34—36

[12] Hu W., Gu J., George Z., Ricketts D.: 'Directed scanning probe nano-manufacturing of lateral ti-$tio_2$-ti junctions for low capacitance mim rectenna diodes'. Proc. 37th Int. Conf. on Micro and Nano Engineering, Berlin, Germany, September 2011

[13] Hu W., Bain J., Ricketts D.: 'In situ quantification of electrical isolation in STM-fabricated $TiO_x$ nanostructures', *Micro & Nano Lett.*, 2012, **7**, (4), pp. 334—336

[14] Breckenridge R.G., Hosler W.R.: 'Electrical properties of titanium dioxide semiconductors', *Phys. Rev.*, 1953, **91**, (4), p. 793

[15] Pawar S.G., Patil S.L., Chougule M.A., Raut B.T., Jundale D.M., Patil V.B.: 'Polyaniline: $TiO_2$ nanocomposites: Synthesis and characterization', *Arch. Appl. Sci. Res.*, 2010, **2**, (2), pp. 194—201

[16] Kellerer H., Wingert L.: 'Deformation of titanium by surface oxidation', *Metall. Mater. Trans. B*, 1971, **2**, (1), pp. 113—115

[17] Vettiger P.: 'The "millipede"-nanotechnology entering data storage', *IEEE Trans. Nanotechnol.*, 2002, **1**, (1), pp. 39—55




doi: 10.1049/mnl.2012.0859